

DESIGN AND ANALYSIS OF MULTICHANNEL TRANSMISSION FILTER BASED ON THE SINGLE-NEGATIVE PHOTONIC CRYSTAL

Chien-Jang Wu^{*}, Min-Hung Lee, and Jun-Zhe Jian

Institute of Electro-Optical Science and Technology, National Taiwan Normal University, Taipei 11677, Taiwan, R.O.C.

Abstract—In this work, the multiple filtering phenomenon in a photonic crystal made of single-negative (SNG) materials is investigated. We consider a finite photonic crystal $(AB)^N$ immersed in air, in which A, B are epsilon-negative (ENG) and mu-negative (MNG) materials, respectively, and N is the stack number. It is found that such a photonic crystal can function as a multichannel transmission filter with a channel number equal to $N - 1$. The required condition is that the thickness of MNG layer must be larger than that of ENG layer when magnetic plasma frequency is greater than electric plasma frequency. The channel frequencies can be red-shifted as the thickness of MNG layer decreases. The channel positions can be tuned by the incidence angle for both TE and TM polarizations. That is, the peak frequency is blue-shifted when the angle of incidence increases. Additionally, the influence of the static permeability of ENG medium and permittivity of MNG medium is also illustrated. The proposed structure can thus be used to design as a tunable multichannel filter which is of technical use in signal processing.

1. INTRODUCTION

In the past decade, the use of photonic crystals (PCs) to design multichannel transmission filters (MTFs) has attracted much attention. MTFs are useful in the dense wavelength multiplexing system which is important in optical communication. A basic feature of an MTF is that there exist multiple transmission peaks in the transmission spectrum. In most cases, transmission peaks are generated within the photonic band gap (PBG) in the photonic band

Received 22 December 2012, Accepted 19 January 2013, Scheduled 23 January 2013

* Corresponding author: Chien-Jang Wu (jasperwu@ntnu.edu.tw).

structure for a PC. There are several filter structures that can exhibit the multiple transmission peaks. A simple multilayer Fabry-Perot resonator (FPR), $(AB)^N D (AB)^N$, can, in general, have a transmission peak [1]. Here, D is the defect layer sandwiched by two finite host PCs of $(AB)^N$. The number of transmission peaks can be increased as the thickness of layer D increases. As a result, an FPR-type multichannel filter is obtainable [2]. Another filter structure is to replace the single defect layer D by a photonic quantum well (PQW), $(CD)^M$, that is, the structure is $(AB)^N (CD)^M (AB)^N$ [3, 4]. The design idea is that a certain photonic passband of $(CD)^M$ must completely overlap with a PBG of $(AB)^N$. Thus, in $(AB)^N (CD)^M (AB)^N$, due to photonic confinement effect, multiple transmission peaks can be produced within the PBG and the number of peaks is just equal to M , the stack number of the PQW. All the above-mentioned filters are based on the PBG engineering, i.e., all transmission peaks are designed to locate within PBG.

In addition to engineering PBG to realize a multichannel filter, the same goal can be reached by engineering photonic passband in a PC containing a negative-permittivity constituent. Examples of such type are superconductor-dielectric PC [5], plasma-dielectric PC [6, 7], semiconductor-dielectric [8]. In this type of MTF, it is not necessary to introduce any defect layer into the PCs, i.e., the filter structure can be simply as $(AB)^N$, or $(AB)^N A$. Here, one of the two constituents, say A, may be superconductor, plasma, or semiconductor. The multiple transmission peaks are shown to locate in the passband of an infinite PC with $N \rightarrow \infty$. In addition, the number of peaks is also directly related to N .

In this work, we report that an MTF can also be obtained by a defect-free PC made of purely single-negative (SNG) media. SNG materials belong to a kind of electromagnetic metamaterials (MTMs), which were first studied early in 1968 by Veselago [9]. SNG materials have two types. One type is called the epsilon-negative (ENG) medium having a negative real part of complex permittivity but with a positive real permeability. The other type called mu-negative (MNG) is that a medium has a negative real part of complex permeability but with a positive real permittivity. There have been reports on the basic and applied researches based on the use of SNG materials [10–15]. Electromagnetic waves in an SNG medium will be evanescent and thus it cannot propagate in the medium. However, waves can propagate in layered structures composed of ENG and MNG media [16–21]. In a one-dimensional SNG PC formed by repeating the ENG-MNG bilayers, it is found that there is an SNG gap which is quite different from the Bragg gap in a usual photonic crystal [22–24]. The SNG gap also

called zero-effective-phase gap originates from the interactions of the forward and backward evanescent waves in the SNG layers. In a recent paper, properties of zero-effective-phase gap in this SNG PC have been experimentally investigated by Chen et al. [25]. This gap will vanish when both the phase-matching and impedance-matching conditions are met simultaneously. In general, the study of PBG belongs to an infinite PC. However, in this work, we are interested in the finite PC and focus in the photonic passband, not the PBG.

The purpose of this paper is to study the transmission property of an SNG-based photonic crystal, $(AB)^N$, where A is an epsilon-negative (ENG) medium and B is a mu-negative (MNG) one. It will be seen that this finite PC can function as an MTF with channel number equal to $N - 1$. The role played by the thickness of the constituent layer is illustrated. It will be shown that an MTF can be obtained for the thickness of MNG layer being larger than that of the ENG layer. We shall demonstrate that the channel frequency can be tuned by the incidence angle for both TE and TM modes in oblique incidence. In addition, the effects of losses and of static permeability and permittivity are also investigated.

2. BASIC EQUATIONS

The structure of SNG PC is depicted in Figure 1. Layers A and B are ENG and MNG media, respectively. By taking the temporal part as $\exp(j\omega t)$ for all fields, the permittivity and permeability for the ENG layer are described by a Drude-like expression, namely [26]

$$\epsilon_A = 1 - \frac{\omega_{ep}^2}{\omega^2 - j\gamma_e\omega}, \quad \mu_A = a, \tag{1}$$

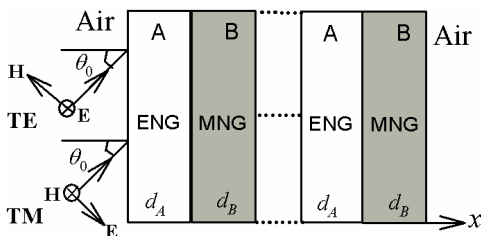


Figure 1. The structure of a photonic crystal $(AB)^N$. Here, A, B are ENG, MNG materials, respectively, and N is the number of periods. A wave with incidence angle θ_0 impinges obliquely on the plane boundary of $x = 0$. Two polarizations, TE and TM waves, are shown.

with $a > 0$. Similarly, the permeability and permittivity for the MNG layer are given by

$$\mu_B = 1 - \frac{\omega_{mp}^2}{\omega^2 - j\gamma_m\omega}, \quad \varepsilon_B = b, \quad (2)$$

with $b > 0$. Here, ω_{ep} and ω_{mp} are electric and magnetic plasma frequencies, respectively. γ_e and γ_m are electric and magnetic damping frequencies, respectively. The refractive indices of ENG and MNG layers are written by

$$n_A(\omega, \gamma_e) = \text{Re}(n_A) - j\text{Im}(n_A) = \sqrt{\varepsilon_A(\omega, \gamma_e)\mu_A}, \quad (3)$$

$$n_B(\omega, \gamma_m) = \text{Re}(n_B) - j\text{Im}(n_B) = \sqrt{\mu_B(\omega, \gamma_m)\varepsilon_B}. \quad (4)$$

In our next analysis, filtering properties of MTF in Figure 1 will be studied through the transmittance T calculated by making use of the transfer matrix method (TMM), with the result [27]

$$T = \left| \frac{1}{M_{11}} \right|^2, \quad (5)$$

where M_{11} is a matrix element of the total transfer matrix given by

$$\mathbf{M} = \begin{pmatrix} M_{11} & M_{12} \\ M_{21} & M_{22} \end{pmatrix} = \mathbf{D}_0^{-1} (\mathbf{D}_A \mathbf{P}_A \mathbf{D}_A^{-1} \mathbf{D}_B \mathbf{P}_B \mathbf{D}_B^{-1})^N \mathbf{D}_0. \quad (6)$$

Here, the dynamical matrix \mathbf{D}_i ($i = 0, A$, and B) is expressed as [28]

$$\mathbf{D}_i = \begin{pmatrix} 1 & 1 \\ \frac{n_i}{\mu_i} \cos \theta_i & -\frac{n_i}{\mu_i} \cos \theta_i \end{pmatrix}, \quad (7)$$

for the TE wave, and

$$\mathbf{D}_i = \begin{pmatrix} \cos \theta_i & \cos \theta_i \\ \frac{n_i}{\mu_i} & -\frac{n_i}{\mu_i} \end{pmatrix}, \quad (8)$$

for the TM wave, respectively. In addition, the propagation matrix \mathbf{P}_i ($i = A, B$) is given by

$$\mathbf{P}_i = \begin{pmatrix} \exp(ik_i d_i) & 0 \\ 0 & \exp(-ik_i d_i) \end{pmatrix}, \quad (9)$$

Note that for $i = 0$, the medium is air. In addition to the transmission spectrum, it is necessary to plot the photonic band structure (PBS) for a PC. If the number of periods N in Figure 1 is infinite, the PBS can be computed by the following equation

$$\begin{aligned} \cos(\phi_{eff}) \equiv \cos(K\Lambda) &= \cos(k_A d_A) \cos(k_B d_B) - \frac{1}{2} \left(\frac{k_A \mu_B}{k_B \mu_A} + \frac{k_B \mu_A}{k_A \mu_B} \right) \\ &\quad \sin(k_A d_A) \sin(k_B d_B), \end{aligned} \quad (10)$$

where K is the Bloch wave number, $\Lambda = d_A + d_B$ is the spatial period, and $k_A = (\omega/c)n_A$, $k_B = (\omega/c)n_B$ are the wave numbers in ENG and MNG layers, respectively. In addition, in the left hand side of Eq. (10), the effective phase or the Bloch phase is defined as $\phi_{eff} = K\Lambda$ [29]. In general, K is complex, i.e., $K = K_r - jK_i$. In the photonic passband, solution for K is purely real whereas it is purely imaginary for the photonic band gap (stop band). It should be mentioned that Eq. (10) is only valid for the case of normal incidence. As for the oblique incidence, Eq. (10) will incorporate the incidence angle and can be expressed in two different forms for the TE and TM waves, respectively [30].

3. NUMERICAL RESULTS AND DISCUSSION

3.1. Effect of Number of Periods

The plasma frequencies in Eqs. (1) and (2) for ENG and MNG media are taken to be $\omega_{ep} = 10$ GHz and $\omega_{mp} = 17.3$ GHz, respectively [31]. Without loss of generality, the damping frequencies are set to be zero, $\gamma_e = \gamma_m = 0$. The effect of damping frequencies will be explored in Subsection 3.4. The inclusion of damping frequencies, in fact, will have a pronounced effect in lowering down the peak height like in the Fabry-Perot resonator [27]. In the absence of damping factor, the frequency will be limited to below 10 GHz in order to make both ϵ_A and μ_B negative.

Figure 2 shows the calculated transmission spectrum for $(AB)^N$ at $N = 2, 3$, and 4, respectively. Here, $d_A = 5$ mm, $d_B = 30$ mm, and $a = b = 1$ are taken. It is of interest to note that there exists certain transmission peak, i.e., the total transmission with $T = 1$. The number of peaks is just equal to $N - 1$. For $N = 2$, there is a single peak with peak frequency at $\omega_1 = 3.4137$ GHz. In addition, the spacing between two adjacent peaks is decreased as N increases. It is expected the number of transmission peaks will be significantly increased at a very large number of N . It is also noted that the frequency range is limited around 3–4 GHz for the all peaks. Combining these properties, at $N \rightarrow \infty$, the infinite discrete peaks will pile together and form a continuous passband shown in Figure 3, which is computed by using Eq. (10). Figure 3 illustrates that, in the frequency region of interest, there exists only a single pass band with band edges marked by two vertical dashed red lines. The left and right band edges are at $\omega_L = 2.9895$ GHz and $\omega_R = 4.1146$ GHz, respectively. Conclusively, the results in Figure 2 reveal that a multichannel transmission filter can be obtained by increasing the stack number N in a finite SNG-based PC.

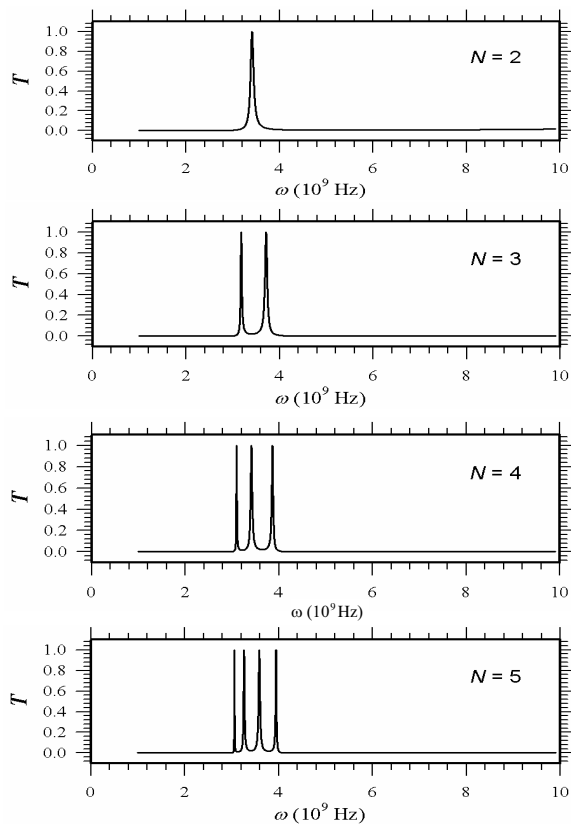


Figure 2. Calculated transmittance spectra for $(AB)^N$ at $N = 2, 3, 4,$ and $5,$ respectively. The number of transmission peaks is $N - 1$ for a given N . Here, $d_A = 5$ mm, $d_B = 30$ mm, and $a = b = 1$.

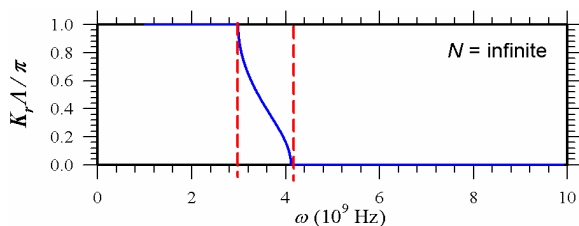


Figure 3. Calculated PBS for $(AB)^N$ at $N \rightarrow \infty$. The band edges are indicated by two vertical dashed lines. Here, $d_A = 5$ mm, $d_B = 30$ mm, and $a = b = 1$.

The appearance discrete resonant transmission peaks can be explored by the theory of thin film optics. The transmittance for $(AB)^N$ can be expressed as [27]

$$T = 1 - R = \frac{\sin^2(\phi_{eff})}{|C|^2 \sin^2(N\phi_{eff}) + \sin^2(\phi_{eff})}, \tag{11}$$

where ϕ_{eff} is given by Eq. (10), and C is one of the matrix elements of the transfer matrix in a single period [27]. The resonant tunneling requires $T = 1$, which in turns leads to

$$\sin(N\phi_{eff}) = 0 \rightarrow \phi_{eff} = \frac{1}{N}s\pi, \quad s = 1, 2, \dots, N - 1, \tag{12}$$

It is worth mentioning that for $s = 0$, there is an additional peak which is not shown in Figure 2. This special mode only exists when the phase-matching condition is met [11, 16]. Now, we try to identify the resonant frequency appearing in Figure 2. First, with Eq. (12), we can calculate the effective phase ϕ_{eff} for every single peak at a given s . Then, with Eq. (10), we can numerically determine the resonant frequency at this s -number. For example, at $N = 2$, we have a single peak with $\phi_{eff} = \pi/2$, which leads Eq. (10) to

$$0 = \cos(k_A d_A) \cos(k_B d_B) - \frac{1}{2} \left(\frac{k_A \mu_B}{k_B \mu_A} + \frac{k_B \mu_A}{k_A \mu_B} \right) \sin(k_A d_A) \sin(k_B d_B), \tag{13}$$

Using the material parameters in Figure 2, the solution for Eq. (13) is calculated to $\omega_1 = 3.41291$ GHz, in good agreement with the first panel of Figure 2. Similarly, for $N > 2$, with Eqs. (10) and (12), we can analytically calculate the peaks frequencies which will be again well consistent with Figure 2.

3.2. Effect of Thicknesses of ENG and MNG Layers

Now let us investigate the effect of thicknesses of ENG and MNG layers on the transmission peaks. In Figure 4, we plot the transmittance spectra for $N = 2$ and $d_A = 5$ mm. The thickness of MNG layer is varied at $d_B = 1, 5, 10, 20, 30$ mm, respectively. Some features are of note. The single peak in the first panel of Figure 2, now in black, is red-shifted as d_B decreases. The peak shape also is broadened. The required narrowband filter is obtained for a thicker MNG layer, say $d_B = 20$ or 30 mm. For $d_B = 1, 5$, and 10 mm, it can be seen that the transmittance is strongly enhanced at frequencies greater than the peak frequency. As a result, the symmetric filtering curve is no longer seen. The red-shift behavior is also seen in the multiple peaks, as illustrated in Figure 5, in which we have considered $N = 3$. In this

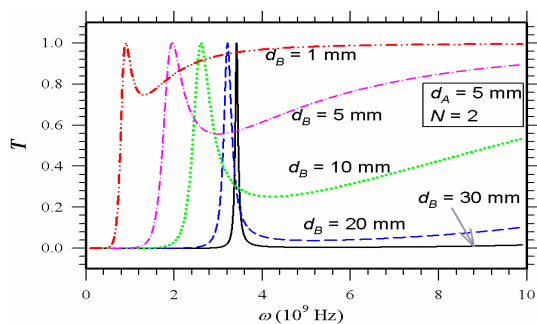


Figure 4. Calculated transmittance spectra for $(AB)^N$ at $N = 2$ and $d_A = 5$ mm for different $d_B = 1, 5, 10, 20,$ and 30 mm, respectively.

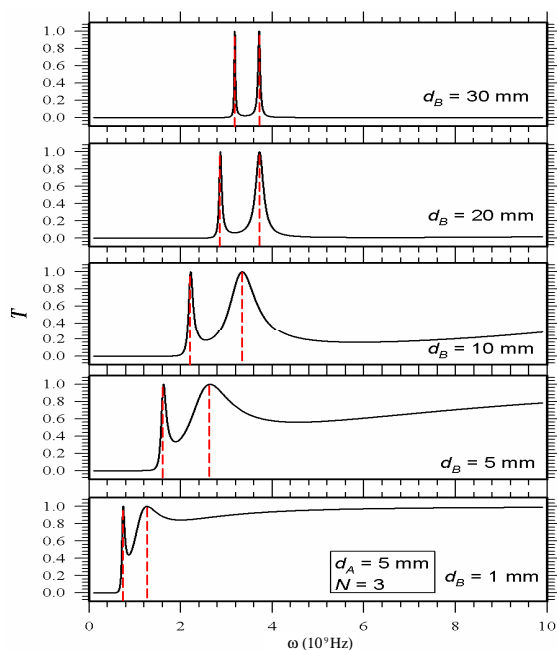


Figure 5. Calculated transmittance spectra for $(AB)^N$ at $N = 3$ and $d_A = 5$ mm for different $d_B = 1, 5, 10, 20,$ and 30 mm, respectively.

case, there are two transmission peaks. The shape of peak at a lower frequency does not change substantially. However, the peak shape at a higher frequency is significantly broadened as in Figure 4.

Taking a close look at Figures 4 and 5 reveals that there exists a cutoff frequency at $d_B = 1, 5,$ and 10 mm because of the absence

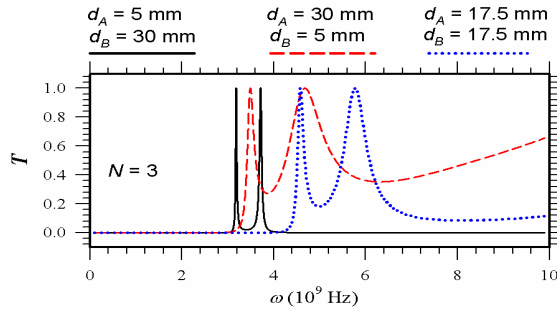


Figure 6. Calculated transmittance spectra for $(AB)^N$ at $N = 3$ with three values in d_A and d_B .

of narrowband filtering feature. At these three thicknesses, the transmission spectra of the structure are continuous at frequency over the cutoff frequency. The cutoff frequency decreases as d_B decreases. In Figure 6, we plot the transmittance at $N = 3$ for three values in $(d_A, d_B) = (5, 30), (30, 5),$ and $(17.5, 17.5)$ mm, respectively. It is seen that the first one $(d_A, d_B) = (5, 30)$ mm is the better condition to achieve the goal of multichannel filter in such an ENG PC. The condition of $(30, 5)$ or $(17.5, 17.5)$ mm will cause the double peaks to be shifted to the higher frequency along with the broadening in their shapes. From the above analysis, we conclude that, in order to obtain the multichannel filter, the thickness of MNG layer must be larger, to some extent, than that of ENG layer.

Before going into the next subsection, we discuss the different choices in the values of $(\omega_{ep}, \omega_{mp})$ in order to obtain the above-mentioned resonant peaks. As indicated in Eqs. (1) and (2), we have taken the Drude-like dispersion expressions for the ENG and MNG materials. These kinds of relations can be realized in special transmission line structures [25, 32]. The values of ω_{ep} and ω_{mp} may be equal or unequal in the literature reports. In the above results, we have taken, $\omega_{ep} < \omega_{mp}$, and the thickness of MNG is required to be larger than that of ENG for the purpose of filtering characteristics. The choice of $\omega_{ep} > \omega_{mp}$ is also available such in Ref. [25]. So, if $\omega_{ep} = 17.3$ GHz and $\omega_{mp} = 10.0$ GHz, we find that, in order to attain the filtering feature, the thickness of ENG has to be larger than that of MNG, as illustrated in Figure 7. Finally, in the case of $\omega_{ep} = \omega_{mp} = 10$ GHz, which has been widely adopted in many reports [33–35], the filtering characteristics can be found when the thickness of ENG is also larger than that of MNG [33].

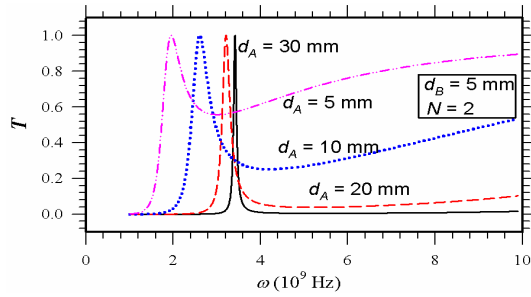


Figure 7. Calculated transmittance spectra for $(AB)^N$ at $N = 2$ and $d_B = 5$ mm for different $d_A = 5, 10, 20,$ and 30 mm, respectively.

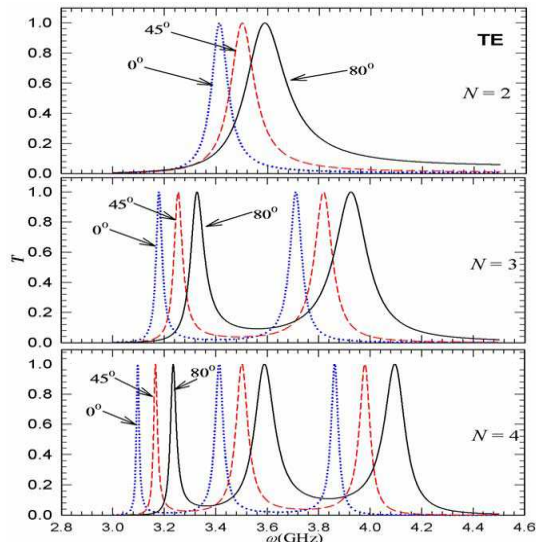


Figure 8. Calculated TE-wave transmittance spectra for $(AB)^N$ at $N = 2, 3,$ and 4 for three different angles of incidence. The peaks are blue-shifted as the angle of incidence increases.

3.3. Effect of Angle of Incidence

We continue to study the effect of angle of incidence layers on the transmission peaks. To illustrate this, it is necessary to consider both TE and TM waves, which have been depicted in Figures 8 and 9, respectively. Here, we plot the PC with $N = 2, 3,$ and 4 at $(d_A, d_B) = (5, 30)$ mm. It can be seen that the transmission peaks will be blue-shifted as the angle of incidence increases. This shifting feature

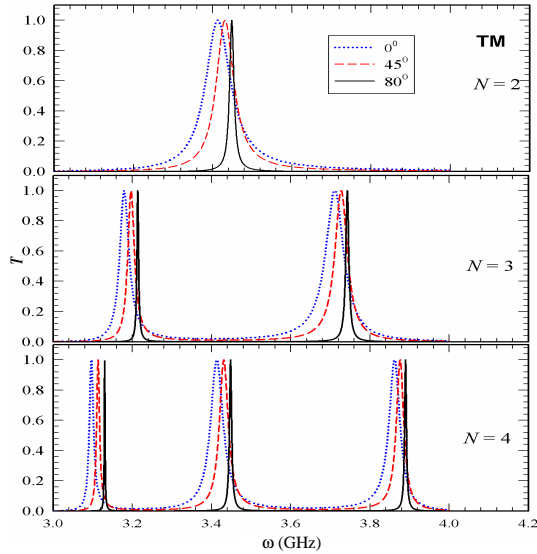


Figure 9. Calculated TM-wave transmittance spectra for $(AB)^N$ at $N = 2, 3,$ and 4 for three different angles of incidence. The blue-shift is not pronounced as in TE wave.

is more salient in the TE wave than TM wave. For TE wave, the peak shape is also broadened in addition to the blue-shift. However, the shape is narrowed down as the angle increases in the TM wave. The results shown here demonstrate that the transmission filter can be tunable as a function of the angle of incidence.

3.4. Effect of Losses in ENG and MNG

Now let us investigate the effect of losses arising from ENG and MNG layers on the transmission peaks. In Figure 10, we plot the normal-incidence transmittance spectra at $N = 3, d_A = 5$ mm, and $d_B = 30$ mm. Here, we have considered four combinations of $(\gamma_e, \gamma_m) = (0, 0), (0, 0.01\omega_{mp}), (0.01\omega_{ep}, 0),$ and $(0.01\omega_{ep}, 0.01\omega_{mp}),$ respectively. It can be seen that the peak frequencies are slightly affected by the inclusion of losses. The left peak is slightly moved to the right and the right peak is slightly shifted to the left. The inclusion of losses has a salient effect, i.e., in the lowering of the peak height. In addition, the low-frequency (left) peak height is lowered down more pronounced compared to the high-frequency (right) peak. With $(\gamma_e, \gamma_m) = (0.01\omega_{ep}, 0.01\omega_{mp}),$ the double-peak shape has been

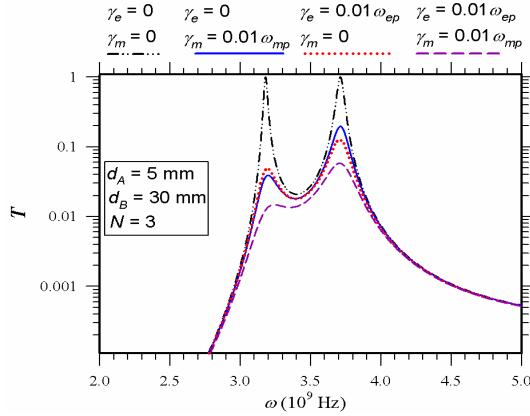


Figure 10. Calculated normal-incidence transmittance spectra for $(AB)^N$ at $N = 3$ in the absence and presence of losses.

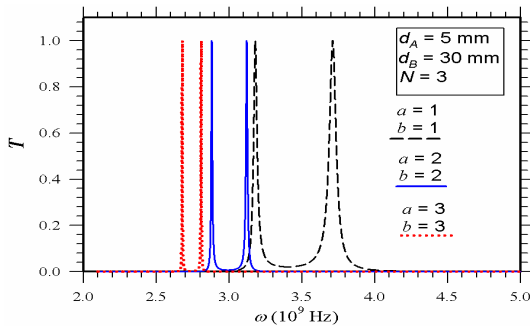


Figure 11. Calculated normal-incidence transmittance spectra for $(AB)^N$ at $N = 3$ with equal values in a and b .

greatly suppressed such that the transmittance is negligibly small. The lowering in the peak height is also seen in the Fabry-Perot resonator when the cavity medium is lossy [27]. In this analysis, we have taken the loss factor which is 0.01 times of the plasma frequency. This choice is only for the illustrative purpose. The real loss factor may be on this order of magnitude or even less than this value [36, 37].

3.5. Effect of Static Positive Parameters (a , b) in ENG and MNG

Let us turn our attention to the effect of static positive parameters (a , b) in Eqs. (1) and (2) on the transmission peaks. Here, a is

the static permeability and b is static permittivity of the ENG and MNG media, respectively. In Figure 11, we plot the normal-incidence transmittance spectra at $N = 3$, $d_A = 5$ mm, and $d_B = 30$ mm. Here, we do not include the losses, and a, b are assumed to be equal, i.e., $a = b = 1, 2$, and 3 are taken. It can be seen from figure that the transmission peaks are red-shifted as the values of a and b increase. The separation between two peaks is also decreased. Additionally, more sharp peaks can be obtained, leading to a preference for the design of a narrowband filter. In fact, the red-shift effect is mainly contributed by the increase in b -value since we have found that transmittance spectra for $(a,b) = (1, 1), (1, 2)$, and $(1, 3)$ are nearly the same as in Figure 11. This may be due to the fact that the thickness of MNG layer is larger than that of ENG one.

3.6. Extended Study on PC Heterostructure, $(AB)^N(BA)^N$

We have thus far given a detailed study on the PC of $(AB)^N$. Before we go to the conclusion, we pay attention to the PC heterostructure (PCH) of $(AB)^N(BA)^N$. With the same parameters in Figures 8 and 9, we plot the transmittance for TE and TM waves in Figures 12 and 13, respectively. It is seen that every single transmission peak has been split into two peaks in the PCH structure. The shifting features for

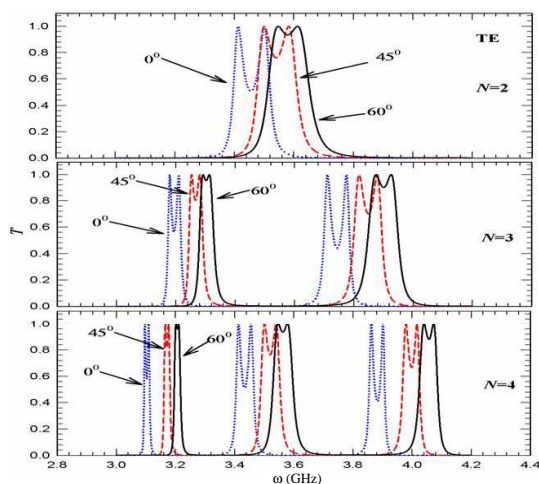


Figure 12. Calculated TE-wave transmittance spectra for $(AB)^N(BA)^N$ at $N = 2, 3$, and 4 for three different angles of incidence. The peaks are blue-shifted as the angle of incidence PCH increases. The original single peak is split into two peaks in the PCH.

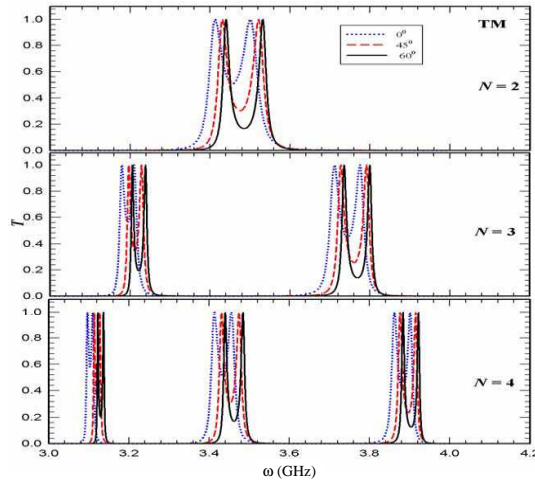


Figure 13. Calculated TM-wave transmittance spectra for $(AB)^N(BA)^N$ at $N = 2, 3$, and 4 for three different angles of incidence. The peaks are blue-shifted as the angle of incidence increases. The original single peak is split into two peaks in the PCH.

TE and TM waves are also very similar to those in Figures 8 and 9. However, the splitting is not so pronounced at a large angle of incidence in the TE wave. The splitting is more salient as the angle of incidence increases in the TM wave.

4. CONCLUSION

Based on the use of an SNG-PC made of ENG-MNG bilayers, a multichannel filter can be achieved at frequencies below the plasma frequencies of both ENG and MNG layers. According to the transmission properties that have been analyzed from the transfer matrix method, some conclusions can be drawn as follows. First, the number of transmission peaks representing the number of filtering channels is shown to be directly determined by the stack number, i.e., $N - 1$. In addition, when N approaches infinite, the infinite discrete peaks will pile together and then a continuous passband is built up. Second, to achieve such a multichannel filter, the thickness of MNG layer is required to be larger than that of ENG layer. The peak frequency is moved to the lower frequency as the thickness of MNG layer decreases. Third, the peak frequency, however, is shifted to the higher frequency as a function of the angle of incidence for both TE

and TM waves. Fourth, the inclusion of losses does not influence the peak frequency, but only lowers down the peak height. Fifth, the effect of static positive parameters on the transmission peaks is also elucidated. Finally, we have investigated the splitting phenomenon in the PCH structure.

ACKNOWLEDGMENT

C.-J. Wu acknowledges the financial support from the National Science Council of the Republic of China (Taiwan) under Contract No. NSC-100-2112-M-003-005-MY3 and from the National Taiwan Normal University under NTNU100-D-01.

REFERENCES

1. Orfanidis, S. J., *Electromagnetic Waves and Antennas*, Chapter 7, Rutgers University, 2008, www.ece.rutgers.edu/~orfanidi/ewa.
2. Wu, C.-J. and Z.-H. Wang, "Properties of defect modes in one-dimensional photonic crystals," *Progress In Electromagnetics Research*, Vol. 103, 169–184, 2010.
3. Qiao, F., C. Zhang, and J. Wan, "Photonic quantum-well structure: Multiple channeled filtering phenomena," *Applied Physics Letters*, Vol. 77, 3698–3700, 2000.
4. Liu, J., J. Sun, C. Huang, W. Hu, and D. Huang, "Optimizing the spectral efficiency of photonic quantum well structures," *Optik*, Vol. 120, 35–39, 2009.
5. Lin, W.-H., C.-J. Wu, T.-J. Yang, and S.-J. Chang, "Terahertz multichanneled filter in a superconducting photonic crystal," *Optics Express*, Vol. 18, 27155–27166, 2010.
6. Li, C., S. Liu, X. Kong, H. Zhang, B. Bian, and X. Zhang, "A novel comb-like plasma photonic crystal filter in the presence of evanescent wave," *IEEE Transactions on Plasma Science*, Vol. 39, 1969–1973, 2011.
7. Wu, C.-J., Y.-J. Lee, T.-C. King, and W.-K. Kuo, "A multichannel filter based on the finite plasma photonic crystal," *Key Engineering Materials*, Vol. 538, 297–300, 2013.
8. Hung, H.-C., C.-J. Wu, T.-J. Yang, S.-J. Chang, "Analysis of tunable multiple-filtering property in a photonic crystal containing strongly extrinsic semiconductor," *Journal of Electromagnetic Waves and Applications*, Vol. 25, Nos. 14–15, 2089–2099, 2011.
9. Veselago, V. G., "The electrodynamics of substances with

- simultaneously negative values of ε and μ ,” *Sov. Phys. Usp.*, Vol. 10, 509–514, 1968.
10. Feng, T., Y. Li, H. Jiang, W. Li, F. Yang, X. Dong, and H. Chen, “Tunable single-negative metamaterials based on microstrip transmission line with varactor diodes loading,” *Progress In Electromagnetics Research*, Vol. 120, 35–50, 2011.
 11. Lin, W.-H., C.-J. Wu, T.-J. Yang, and S.-J. Chang, “Analysis of dependence of resonant tunneling on static positive parameters in a single-negative bilayer,” *Progress In Electromagnetics Research*, Vol. 118, 151–165, 2011.
 12. Radi, Y., S. Nikmehr, and S. Hosseinzadeh, “A rigorous treatment of vertical dipole impedance located above lossy DPS, MNG, ENG, and DNG half-space,” *Progress In Electromagnetics Research*, Vol. 116, 107–121, 2011.
 13. Petrillo, L., F. Jangal, M. Darces, J.-L. Montmagnon, and M. Hélier, “Negative permittivity media able to propagate a surface wave,” *Progress In Electromagnetics Research*, Vol. 115, 1–10, 2011.
 14. Ng Mou Kehn, M., “Spherical slotted antenna coated with double layer of materials having combinations of singly and doubly negative parameters and consequences of mode resonances,” *Progress In Electromagnetics Research B*, Vol. 45, 223–249, 2012.
 15. Liu, C.-H. and N. Behdad, “Theoretical examination of electromagnetic wave tunneling through cascaded ϵ - and μ -negative metamaterial slabs,” *Progress In Electromagnetics Research B*, Vol. 42, 1–22, 2012.
 16. Alu, A. and N. Engheta, “Pairing an epsilon-negative slab with a mu-negative slab: Resonance, tunneling and transparency,” *IEEE Transactions on Antenna Propagation*, Vol. 51, 2558–2571, 2003.
 17. Castaldi, G., I. Gallina, V. Galdi, A. Alu, and N. Engheta, “Electromagnetic tunneling through a single-negative slab paired with a double-positive bilayer,” *Physical Review B*, Vol. 83, 081105(R), 2011.
 18. Cojocar, E., “Electromagnetic tunneling in lossless trilayer stacks containing single-negative metamaterials,” *Progress In Electromagnetics Research*, Vol. 113, 227–249, 2011.
 19. Feng, T., Y. Li, H. Jiang, Y. Sun, L. He, H. Li, Y. Zhang, Y. Shi, and H. Chen, “Electromagnetic tunneling in a sandwich structure containing single negative media,” *Physical Review E*, Vol. 79, 026601, 2009.
 20. Ding, Y. Q., Y. H. Li, H. T. Jiang, and H. Chen, “Electromagnetic

- tunneling in nonconjugated epsilon-negative and mu-negative metamaterial pair,” *PIERS Online*, Vol. 6, No. 2, 109–112, 2010.
21. Fredkin, D. R. and A. Ron, “Effective left-handed (negative index) composite material,” *Applied Physics Letters*, Vol. 81, 1753–1755, 2002.
 22. Wang, L. G., H. Chen, and S. Y. Zhou, “Omnidirectional gap and defect mode of one-dimensional photonic crystals with single-negative materials,” *Physical Review B*, Vol. 70, 245102, 2004.
 23. Yeh, D.-W. and C.-J. Wu, “Analysis of photonic band structure in a one-dimensional photonic crystal containing single-negative material,” *Optics Express*, Vol. 17, 16666–16680, 2009.
 24. Yeh, D.-W. and C.-J. Wu, “Thickness-dependent photonic bandgap in a one-dimensional single-negative photonic crystal,” *Journal of Optical Society of America B*, Vol. 26, 1506–1510, 2009.
 25. Chen, Y., X. Wang, Z. Yong, Y. Zhang, Z. Chen, L. He, P. F. Lee, H. L. W. Chan, C. W. Leung, and Y. Wang, “Experimental investigation of photonic band gap in one-dimensional photonic crystals with metamaterials,” *Physics Letters A*, Vol. 376, 1396–1400, 2012.
 26. Lin, W.-H., C.-J. Wu, and S.-J. Chang, “Angular dependence of wave reflection in a lossy single-negative bilayer,” *Progress In Electromagnetics Research*, Vol. 107, 253–267, 2010.
 27. Yeh, P., *Optical Waves in Layered Media*, John Wiley & Sons, Singapore, 1991.
 28. Lin, W.-H., C.-J. Wu, and S.-J. Chang, “Analysis of angle-dependent unusual transmission in lossy single-negative (SNG) materials,” *Solid State Communications*, Vol. 150, 1729–1732, 2010.
 29. Jiang, H., H. Chen, H. Li, Y. Zhang, J. Zi, and S. Zhou, “Properties of one-dimensional photonic crystals containing single-negative materials,” *Physical Review E*, Vol. 69, 066607, 2004.
 30. Depine, R. A., M. L. Martínez-Ricci, J. A. Monsoriu, E. Silvestre, and P. Andrés, “Zero permeability and zero permittivity band gaps in 1D metamaterial photonic crystals,” *Physics Letters A*, Vol. 364, 352–355, 2007.
 31. Dong, L., G. Du, H. Jiang, H. Chen, and Y. Shi, “Transmission properties of lossy single-negative materials,” *Journal of Optical Society of America B*, Vol. 26, 1091–1096, 2009.
 32. Eleftheriades, G. V., A. K. Iyer, and P. C. Kremer, “Planar negative refractive index media using periodically L-C loaded

- transmission lines,” *IEEE Transactions on Microwave Theory and Technology*, Vol. 50, 2702–2712, 2002.
33. Li, P. and Y. Liu, “Multichannel filtering properties of photonic crystals consisting of single-negative materials,” *Physics Letters A*, Vol. 373, 1870–1873, 2009.
 34. Rahimi, H., “Backward Tamm states in 1D single-negative metamaterial photonic crystals,” *Progress In Electromagnetics Research Letters*, Vol. 13, 149–159, 2010.
 35. Shi, L., S. Wang, C. Tang, and L. Gao, “Omnidirectional surface guided modes from one-dimensional photonic crystal formed by single-negative materials,” *Journal of Magnetism and Magnetic Materials*, Vol. 311, 609–613, 2007.
 36. Chen, Y., Y. Wang, C. W. Leung, M. Hu, and H. L. W. Chan, “Photonic gap vanishing in one-dimensional photonic crystals with single-negative metamaterials,” *Physics Letters A*, Vol. 375, 2465–2470, 2011.
 37. Wang, L.-G., H. Chen, and S.-Y. Zhou, “Wave propagation inside one-dimensional photonic crystals with single-negative materials,” *Physics Letters A*, Vol. 350, 410–415, 2006.